Memories of the Faculty of Science, Kyoto University, Series of Physics, Astrophysics, Geophysics and Chemistry Vol. XXXVII, No. 3, Article 1, 1989

MEASUREMENT OF TOTAL CROSS SECTIONS OF MULTIHADRON PRODUCTION FOR e^+e^- ANNIHILATION AT $\sqrt{s}=50$ AND 52 GeV

By

Yoshikazu YAMADA*

Department of Physics, Faculty of Science, Kyoto University, Kyoto 606, Japan

(Received January 6, 1988)

Abstract

The total cross section of multi-hadron production for the e^+e^- annihilation and the R ratio at $\sqrt{s}=50$ and 52 GeV have been measured with an accuracy of 7% with the VENUS detector in TRISTAN. The results are consistent with the predictions basing on five known quarks of u, d, s, c and b. The production of the open top quark is excluded with the confidence level of 95%. The Weinberg angle of $\sin^2\theta_W$ evaluated from the R ratios is $0.26\pm 0.04\pm 0.06$.

1. INTRODUCTION

In the last two decades, the standard model which can describe the properties of the elementary particles and the fundamental interactions has been developed in the framework of $SU(3)_{\text{color}}\otimes SU(2)_L\otimes U(1)$ model with the quark parton picture [1, 2], and it has been found that the standard model can explain many experimental results without any contradictions. Among these experiments, the experiments on the electron positron annihilation have played an important role not only for the development of the standard model but also for the discoveries of new quarks and leptons. The first succession of the e^+e^- collider is the discovery of the very narrow resonance named J/ψ at SPEAR in 1974 [3] at the same time as the discovery of the narrow e^+e^- resonance in the 30 GeV proton-nucleus collision at BNL [4]. It was interpreted as the bound state of a new fourth quark-antiquark pair named charm (c) which had been predicted by the GIM mechanism [5] based on the unified electroweak theory. Subsequently, a pair production of new heavy lepton named τ was discovered at SPEAR in 1975 in anomalous e–μ events [6]. τ was interpreted as a sequential lepton with its neutrino ν_τ from the conservation law of lepton numbers. Then the new resonance called Υ was found in the $\mu^+\mu^-$ pair production at FNAL in 1977 [7], and it was soon established with its exited states at DORIS in 1978 [8]. They were interpreted as the bound states of a new fifth quark-antiquark pair named bottom (b).

From these discoveries and subsequent studies of their decay processes, the idea

* Now at the National Laboratory for High Energy Physics, Tsukuba 305, Japan.

of the generation and mixing were established to understand the weak interactions of quarks and leptons. Known 6 leptons and 5 quarks are classified into 3 generations as (ν_e, e), (ν_μ, μ), (ν_τ, τ) for leptons and (u, d), (c, s), (b) for quarks. In spite of continuous searches with e^+e^- colliding machines such as SPEAR/DORIS and PETRA/PEP, the top quark expected to belong to the same generation of the b quark has not been found [9].

With e^+e^- colliding machines, we can test the existence of the new quark and/or the validity of the standard model by measuring the total cross section of multi-hadron production for e^+e^- annihilation. According to the standard model, a e^+e^- pair annihilates into γ or Z^0, then they are converted into a quark-antiquark pair. The quark and antiquark are fragmented into multi-hadrons. Therefore, the cross section of multi-hadron production depends on the number of quark flavors. However, this cross section has the $1/s$ ($s=(CM\ energy)^2$) dependence. The following R ratio which is almost free from the s dependence was introduced,

$$R \equiv \frac{\sigma(e^+e^- \to (\gamma/Z^0)^* \to hadrons)}{\sigma_{point}} \tag{1}$$

$$= \sum_q 3Q_q^2 \times (1+C_{QCD}) \times (1+C_{Weak}) , \tag{2}$$

with

$$\sigma_{point} = \frac{4\pi\alpha^2}{3s} ,$$

where σ_{point} represents the point like QED cross section of fermion pair production. Q_q is the quark charge normalieed by $|e|$. The factor $\sum_q 3Q_q^2$ is expected from the naive colored quark parton model. The factors $1+C_{QCD}$ and $1+C_{Weak}$ are the correction factors by QCD and the weak interactions, respectively.

If the top quark having the charge of $2/3 \times |e|$ exists, the R ratio should increase by about $3 \times (2/3)^2 = 4/3$ from the value which is expected from the production of the five known quarks. The R ratio has been measured extensively with SPEAR/DORIS and PETRA/PEP up to $\sqrt{s}=46.7$ GeV, and is about 3.8 which agrees with the expected value with five quarks. These results show no indication of the existence of the top quark in this energy region.

In the energy region above 40 GeV, the e^+e^- annihilation into Z^0 becomes appreciable, so that C_{Weak} is expected to be 0.2. This gives a chance to measure the Weinberg angle $\sin^2\theta_W$ which determines the weak coupling of quarks and leptons, as will be discussed in Section 4.3.

In order to search the top quark and to develop the standard model in the world highest energy region, a 30 GeV+30 GeV e^+e^- colliding machine called "TRISTAN" [10], which stands for Transposable Ring Intersecting STorage Accelerator in Nippon, was constructed at KEK (NLHEP: National Laboratory for High Energy Physics) in Japan. Fig. 1 shows the layout of TRISTAN. Three detectors called VENUS, TOPAZ and AMY were also constructed at the long straight sections.

TRISTAN succeeded to make e^+e^- collisions at 25 GeV+25 GeV in November

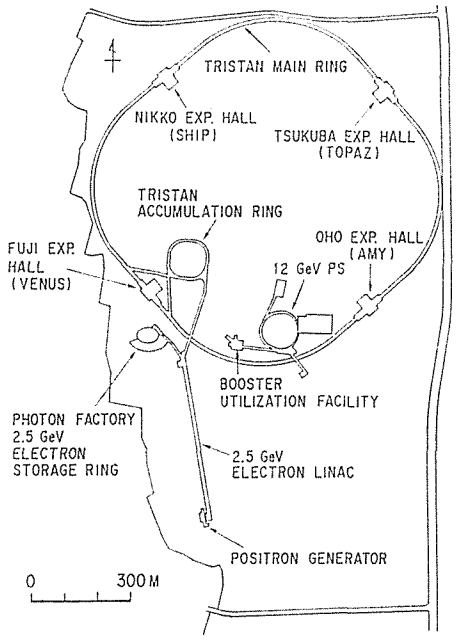

Fig. 1. Layout of TRISTAN

1986. The experiment started in January 1987, then in June 1987, the energy of TRISTAN increased up to 26 GeV+26 GeV.

This paper reports the results of the measurement of the total cross section of multi-hadron production with the VENUS detector at $\sqrt{s}=50$ and 52 GeV.

2. APPARATUS

2.1. TRISTAN

TRISTAN consists of three accelerators. Positrons are produced by a 200 MeV electron linac and accelerated by a 250 MeV positron linac. Then positrons are fed into the 2.5 GeV linac (LINAC used for KEK Photon Factory). The positrons of 2.5 GeV are injected into the Accumulation Ring (AR; 8 GeV synchrotron) and accelerated up to 7.3 GeV, and fed into the Main Ring (MR; 30 GeV synchrotron). Electrons are accelerated up to 2.5 GeV by LINAC and injected into AR. The electrons are also accelerated up to 7.3 GeV and fed into MR. Finaly electrons and positrons are accelerated to the final beam energy. A typical filling time to MR is 30 minutes.

MR is 3 km in circumference and has four long straight sections of 193 m where the high power RF stations are located. The bending radius R is 246 m, so that the synchrotron radiation loss is rather high. Therefore, the energy spread of beams σ_E expressed as

$$\sigma_E/E = 0.857\times10^{-3}\times E_{beam}(\mathrm{GeV})/R(\mathrm{cm})$$

amounts to 49 MeV at 30 GeV.

TRISTAN is designed to accumulate the electron and positron beams of 10 mA, and is expected to provide the luminosity of

$$L \approx 2 \times 10^{31}\,\mathrm{cm}^{-2}\,\mathrm{sec}^{-1}\,.$$

At present, the beam current is lower than the design value due to the beam instability in MR and limits our luminosity. During the data taking run of the present experiment, the average luminosity was

$$L \approx 4 \times 10^{30}\,\mathrm{cm}^{-2}\,\mathrm{sec}^{-1}\,.$$

2.2. VENUS Detector

The VENUS detector, which stands for VErsatile Nlhep and Universities Spectrometer, is a general purpose magnetic spectrometer with electromagnetic calorimeters [11]. Its main features are to have a large angular coverage both for charged and neutral particles with good spatial and energy resolutions and to be constructed with well established techniques. As is shown in Fig. 2, it consists of a inner chamber, a central drift chamber, outer drift tubes, time of flight counters, a superconducting solenoid, limited streamer tubes, lead glass and liquid argon calorimeters, muon chambers and luminosity monitors. The inner chamber, central drift chamber and outer drift tubes are used for tracking the charged particles and for measuring their momenta. The lead glass and liquid argon calorimeters are used to measure the energy of electrons and gammas in the large angles and forward angles, respectively.

In this analysis, the z axis is chosen to be the direction of electrons, and the direction of x axis is chosen in the outward direction from MR.

1. Beam pipe

   The beam pipe is made of 3 mm thick aluminum having a inner radius of

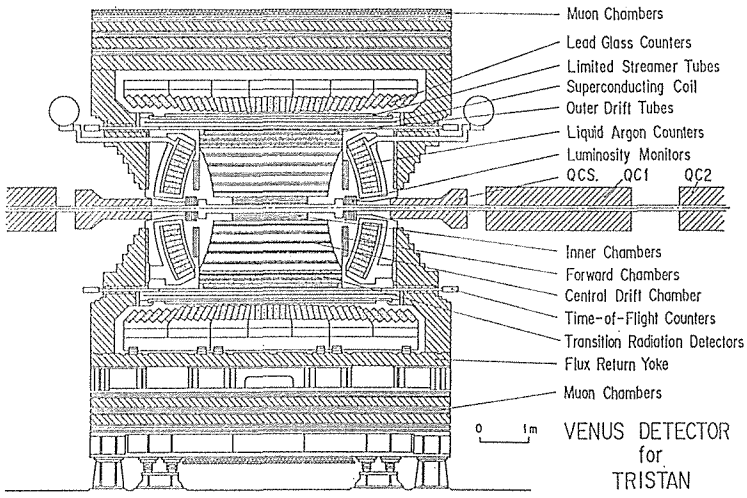

Fig. 2. Side view of the VENUS detector

90 mm. The vacuum at the interaction point has been kept below 10^{-8} Torr.

2. Inner chamber (IC)
The inner chamber (IC) is a cylindrical multiwire drift chamber of 6 layers. The inner and outer radii are 10 and 25 cm, respectively. The length is 160 cm. The anode wires measure the r-ϕ coordinates and the cathode pads measure the z coordinates. The HRS gas ($Ar(89\%)/CO_2(10\%)/CH_4(1\%)$) is filled in the chamber. The cathode pads of 18 μm thick copper are plated on a Kapton sheet of 125 μm. These Kapton sheets are glued on the "paper honeycomb" cylinder in order to minimize the multiple scattering and photon conversion in the chamber. The signals from cathode pads are amplified by pre-amplifiers placed on the end plates and are latched by discriminators in the TKO [12] (Tristan Kek Online) box. By using the "Memory Look-up Table", the combination of signals generates a fast z-trigger signal for selecting the events originated from the interaction points. This fast z-trigger efficiently rejects a large amount of backgrounds such as the beam-gas interaction and cosmic rays. The details of IC are given in Ref. [13]. However, during the period of the present experiment, the fast z-trigger was not operated because of the heavy background from the halo beam around IC.

3. Central drift chamber (CDC)
The central drift chamber (CDC) is placed outside the inner chamber [14]. CDC is the cylindrical multiwire drift chamber which has 20 layers of axial wires for measuring the r-ϕ coordinates and 9 layers of stereo wires. The stereo wires have an angle of 3.3° with respect to the z-axis for measuring the z coordinates. The inner and outer radii are 25 and 126 cm, respectively. The length is 300 cm. The chamber is filled by the HRS gas. In the range of polar angles from 40° to 140°, twenty r-ϕ coordinates are measured along each track. Both the inner and outer cylinders are made of CFRP of 1 mm and 5 mm thick, respectively. The end plate is a 2.1 cm thick aluminum disc. The anode wires are 30 μm-ϕ tungsten wires plated by gold, while the potential wires are 140 μm-ϕ molybdenum wires plated by gold. Two axial layers and one stereo layer are combined into one group. A pair of axial layers are staggered by a half of the cell width. These staggered layers are used to solve the left-right ambiguity within one group. Signals from anode wires are amplified by pre-amplifiers placed on the end plate and transmitted to the discriminators and TAC-ADC system on FASTBUS [15]. Signals from the discriminators are also fed to the track-finder module on FASTBUS and used to generate a fast r-ϕ trigger signal by the aid of memory look-up tables. The spatial resolution of this system was evaluated to be about 200 μm from the measurement of cosmic rays. The momentum resolution was found to be $\sigma_P/P=\sqrt{(1\%)^2+(0.6\%\times P(\mathrm{GeV/c}))^2}$ at $B=7.5$ kG from the measurement of Bhabha scattering, where P is the momentum of the particle

in the unit of GeV/c.

4. Time of flight counter (TOF)
   The time of flight counter system [16] for particle identification consists of 96 plastic scintillators of KYOWA SCSN-23. Each scintillator is viewed through a light guide by phototubes (HAMAMATSU H1949) at both end. The counter size is 10.8 cm wide, 4.2 cm thick, and 466 cm long. These counters are mounted on the inner wall of the superconducting solenoid at the radius of 166 cm from the beam axis. Signals from phototubes are transmitted to the discriminators and TDC-ADC system in the TKO box. This system is monitored by a laser calibration system. At the present stage, the time resolution of this system is about 400 psec from the measurement of the μ pair production. $\pi^{\pm}$'s and protons below 1 GeV/c are clearly identified as shown in Fig. 3. The time resolution is being improved by using the informations of pulse heights measured by ADC's. Signals from discriminators are also fed to the trigger decision module on FASTBUS in order to eliminate the cosmic ray background by setting a time window of 150 nsec after the beam crossing time. The details of the TOF system will be described in Appendix A.
5. Superconducting solenoid
   A superconducting thin solenoid magnet was employed to produce a uniform magnetic field of 7.5 kG in a volume of 3.4 m in diameter and 5.2 m in length by keeping the coil as thin as possible to minimize the energy losses of particles through the coil [17]. The thickness of the solenoid magnet including the encloser is 20 cm, while the effective thickness is 0.64 radiation lengths. The coil is made of superconducting cables which contain a Nb-Ti/Cu multifilamentary superconducting composite in a pure aluminum stabilizer. The

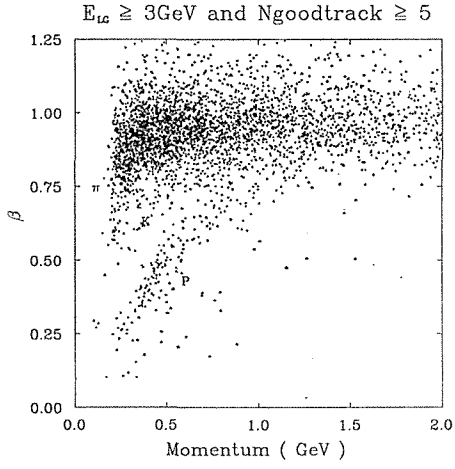

Fig. 3. Scattered plot of the momentum versus β for the selected events.

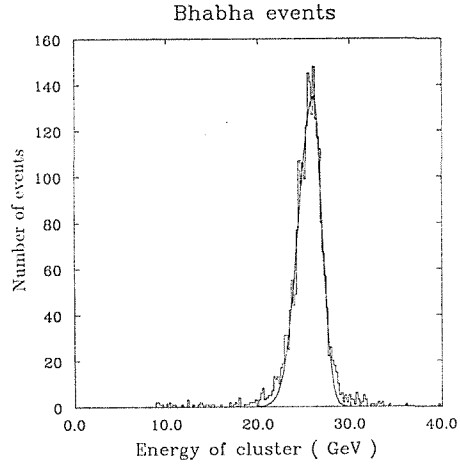

Fig. 4. Energy distribution of the lead glass calorimeter for Bhabha scattering events at $E_{beam}=26$ GeV.

coil is supported not by a bobbin but by a case outside the coil winding. The magnet is cooled by the two phase helium flow in the cooling path made in the coil case. The magnetic field is uniform within 1% in the volume of CDC. The leakage field outside the coil was measured to be less than 35 gauss.

6. Barrel lead glass calorimeter (LG)
   The barrel lead glass calorimeter (LG) [18] is placed between the superconducting coil and the return yoke to measure the energies of electrons and gammas. LG covers polar angles from 37° to 143°. LG is segmented into 120 in the ϕ-view and 43 in the θ-view, so that all together 5160 blocks of lead glass of NIKON SF6 are mounted in place. Each lead glass block is approximately pointing to the interaction region in order to reduce the systematic error of energy measurement due to the shower leakage into adjacent blocks. The size of each block is 12.0 cm wide, 11.6 cm high, and 30.4 cm long having 18 radiation lengths. Each block is viewed by a 3″ diameter phototube (HAMAMATSU R1911) through a acryl light guide of 6 cm long. All counters are arranged to form 58 groups for the trigger purpose. The signals from 5160 counters are read out by 96 channel 12 bit ADC's (LeCroy 1880 system) on FASTBUS. Each ADC module consisting of 96 channels produces an analogue sum signal, then those sum signals are further summed up to give the total energy sum signal and the segment sum signals for 58 groups of the segments. These sum signals were used for the energy trigger in the trigger system. The energy resolution was evaluated to be $\sigma_E/E=1\%+7\%/\sqrt{E(\mathrm{GeV})}$ from the measurement of the Bhabha scattering as shown in Fig. 4.
7. Endcap liquid argon calorimeter (LA)
   Two liquid argon calorimeters (LA) for measuring the energies of electrons and gammas are placed between CDC and both endcaps of the magnet. Each calorimeter covers polar angles from 8°(143°) to 37°(172°). However, the construction of LA was so delayed that LA was not operated during the period of the present experiment.
8. Muon chamber
   The muon chamber system [19] consists of 6 layers of drift tubes interleaved with thick iron absorbers placed outside of the return yokes and it covers 84 % of the whole solid angle. Only a part of the system was installed during the period of the present experiment.
9. Luminosity monitor (LM)
   The luminosity monitor (LM) consists of 27 layers of lead sheets and scintillators totaling 20 radiation lengths. The shape is cylindrical, and the inner and outer radii are 7 cm and 24 cm, respectively. LM covers polar angles from 47 m radians to 140 m radians. Each calorimeter is divided into 8 pieces in the xy-plane and back to back signals in three dimensional space are used for triggering the small angle Bhabha scattering. Lights from

scintillators are collected by wavelength-shifter-bars at both sides of the scintillators and are guided to the phototubes of Hamamatsu R2114. Signals from phototubes are transmitted to 12 bit ADC's (LeCroy 1880 system) on FASTBUS. The energy resolution was evaluated to be $\sigma_E/E=37\%/\sqrt{E(\mathrm{GeV})}$ from the measurement of the Bhabha scattering.

2.3. Trigger and Data Acquisition

2.3.1. Trigger System

In the main ring, electrons and positrons collide every 10 μsec, but the e^+e^- interaction rate is very low due to its very small cross section. An efficient trigger system is necessary in order to select the events which originate from the e^+e^- interactions, so as to reject a large amount of backgrounds such as beam–residual gas, beam–beam pipe interactions and cosmic rays. The main features of our trigger system [20] are the fast decision within each beam crossing and the flexibility by using the memory look-up tables. The following informations were available for the fast trigger system.

(a) Track informations
Tracks with $P_{xy}\geq 0.7$ GeV are recorded in CDC by using the look-up table in the fast track finder (TF) modules which include 256 piece of 4 k-bit RAM's, where P_{xy} is the transeverse momentum with respect to the beam axis [21].

(b) Energy deposit informations
The total energy deposit in LG and the energy deposit in each 58 groups of LG segments. The thresholds for these energys can be set up at desired values.

These trigger informations are combined by the following trigger conditions.

T1: Total energy deposit of LG is greater than 5 GeV.

T2: At least two tracks are recorded in CDC by TF and at least one of energy deposits in groups of LG is greater than 0.7 GeV.

T3: Two tracks having the angle within 10° each other in the xy-plane (back to back configuration) and the two tracks hit the TOF counters.

Digitizations in the electronics such as TDC and ADC are started by every beam crossing signal. If none of above trigger conditions are satisfied, all digitizing electronics are cleared automatically before the next beam crossing. If one of the trigger conditions are satisfied, the trigger signal masks the next clearing signals. With these trigger conditions, the informations from all the detectors are read by the data acquisition system. The trigger rate depended on the beam conditions, and was about 3 Hz on an average.

2.3.2. Data Acquisition System

Signals from the front-end electronics are digitized by FASTBUS, CAMAC and TKO modules. All together, there consist of 18k channels of FASTBUS modules, 1k channels of CAMAC modules and 11k channels of TKO modules. All the data are transfered to FASTBUS memory buffers and read by an on-line computer of

Table 1 Summary of data taking run

Date	Run number	CM energy	No. of triggers	Integrated luminosity
87/1~87/3	264~ 478	50 GeV	1427707	86 nb^{-1}
87/5~87/6	510~ 692	50 GeV	1622098	609 nb^{-1}
87/6~87/7	704~1076	52 GeV	4568560	2912 nb^{-1}

VAX11–780 through the FASTBUS–VAX interface (VAX–FPI) [22]. A typical data siee is about 5k bytes per event and it takes about 23 msec to read the data into VAX11–780. VAX11–780 is linked to the main computer of FACOM–M382 by 1 km-long optical fiber cables. The data are transfered to FACOM–M382 with a speed of 300k bytes per second and recorded on magnetic cassette tapes.

2.3.3. Summary of Data Taking Run

The data were collected in January and May, 1987, at $\sqrt{s}=50$ GeV, then in June at $\sqrt{s}=52$ GeV. The summary of data taking run is seen in Table 1.

3. DATA ANALYSIS

3.1. Background Reduction

In order to reduce the background such as the beam-beam pipe interaction, beam-gas interaction, and cosmic rays, at first we required the following condition in the data reduction.

i) $E_{LG} \geq 3$ GeV,
where E_{LG} is the total energy deposit in the barrel lead grass calorimeter.

Fig. 5 shows the E_{LG} distribution for all triggered events. A large amount of beam backgrounds and cosmic rays are reduced by this $E_{LG} \geq 3$ GeV cut. The reduction factor of this cut is about 3.0×10^{-2}. The dashed line indicates the E_{LG} distribution of the finally selected multi-hadronic events. It shows that the $E_{LG} \geq 3$ GeV cut is

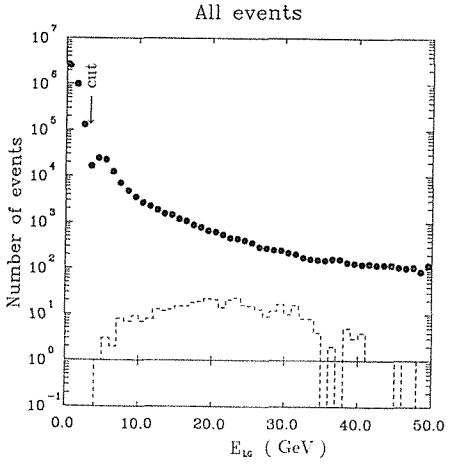

Fig. 5. E_{LG} distribution for all triggered events (●) and for the finally selected multi-hadronic events (dashed line).

safe enough for the multi-hadronic events.

In addition to the $E_{LG} \geq 3$ GeV cut, the following condition was required to select the events.

ii) $N_{track} \geq 2$,
where N_{track} denotes the number of "track"s.

The pattern recognition was made to find the charged tracks in CDC for each events [23]. A charged track satisfying the following conditions was accepted as the "track".

a) The track must be reconstructed in three dimensions.

b) $N_{hit-xy} \geq 8$ and $N_{hit-rz} \geq 4$,
where N_{hit-xy} is the number of hits on axial wires and N_{hit-rz} is that on stereo wires.

c) $|d_{r0}| \leq 3$ cm and $|d_{z0}| \leq 30$ cm,
where d_{r0} is the radius and d_{z0} is the z coordinate at the closest approach to the beam axis.

d) $P_{xy} \geq 0.2$ GeV/c,
because the particles with the momentum less than 0.2 GeV/c move on a circle inside the magnetic field and can not pass through the magnet.

The distributions of N_{hit-xy}, N_{hit-rz}, d_{r0}, and d_{z0} for the finally selected multi-hadronic events are shown in Fig. 6 and 7. It is seen that these conditions do not reject the

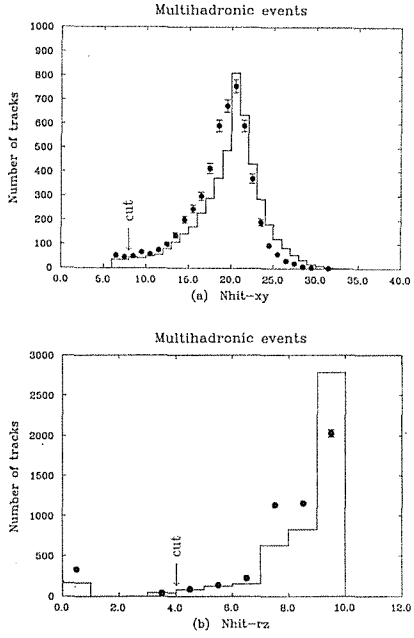

Fig. 6. Number of hits on axial wires (a) and on stereo wires (b) of the tracks for the selected multi-hadronic events (●). The solid lines show the results of the simulations.

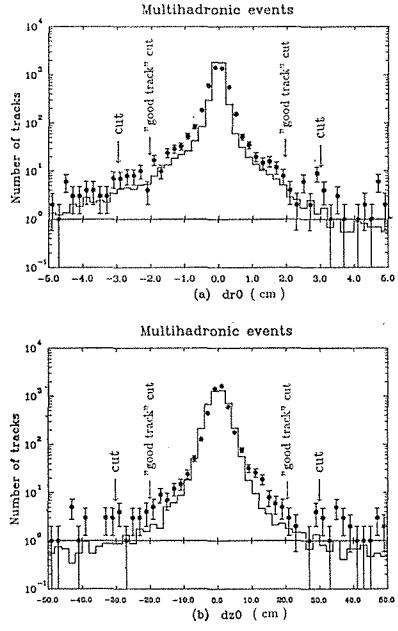

Fig. 7. d_{r0} (a) and d_{z0} (b) distributions of the tracks for the selected multi-hadronic events (●). The solid lines shows the results of the simulation.

wanted multi-hadronic events.

This $N_{track} \geq 2$ cut reduced a large amount of backgrounds from the beam-beam pipe and gas interactions and and the cosmic rays which do not come from the interaction point. The reduction factor of this cut is about 3.0×10^{-2}.

3.2. Selection of the Multi-hadronic Event

The events which pass through the above two cuts still contained many background such as from the cosmic rays, Bhabha scattering, and tau pair productions etc.. Therefore, we required much severe conditions to the events so as to reduce the background.

i) $N_{goodtrack} \geq 5$,
where $N_{goodtrak}$ denotes the number of "good track"s.
The "good track" satisfies the conditions of $|d_{r0}| \leq 2$ cm and $|d_{z0}| \leq 20$ cm, which is much servere than the condition of c) in the previous section.

Fig. 8 shows the $N_{goodtrack}$ distribution of the remaining events after the background reduction mentioned in the previous section. This cut also reduced a large amount of low multiplicity background such as the Bhabha scattering and tau pair production etc.. The solid line indicates the results of the Monte Carlo simulation, and shows that this cut eliminates only the small amount of the multi-hadronic events. The numbers of the remaining events after the cut are 161 events at $\sqrt{s}=50$ GeV, and 673 events at $\sqrt{s}=52$ GeV.

Finaly, we require the following condition which is sensitive to reject the two photon background.

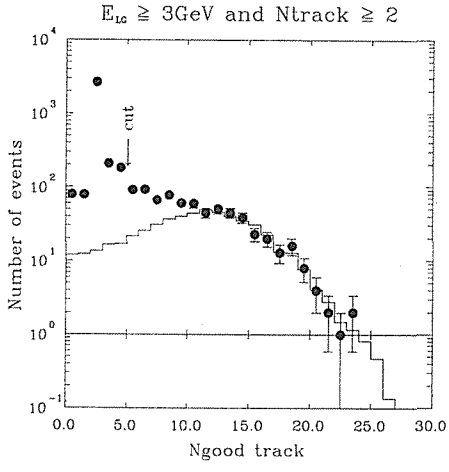

Fig. 8. Number of "good track"s for the events with $E_{LG} \geq 3$ GeV and $N_{track} \geq 2$ (●). The solid line shows the result of the simulation.

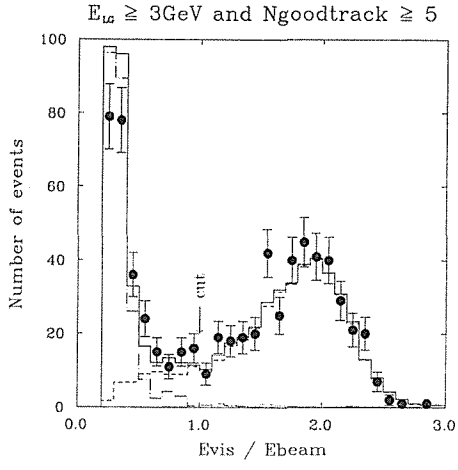

Fig. 9. E_{vis}/E_{beam} distribution for the events after the $E_{LG} \geq 3$ GeV and $N_{goodtrack} \geq 5$ cuts (●). The dashed line indicates the result of the simulation for the multi-hadronic events. The dot-dashed line is the result of the simulation for the two photon interaction.

ii) $E_{vis} \geq E_{beam}$,
where E_{vis} is the total visible energy and is defined as

$$E_{vis} \equiv P_{CDC} + E_{LG},$$

where P_{CDC} is the sum of momenta of all tracks measured by CDC.

Fig. 9 shows the E_{vis}/E_{beam} distribution of the remaining events after above cut. The dashed line indicates the results of the Monte Carlo simulation for the multi-hadronic events performed with LUND 5.3 [24]. The dot dashed line indicates that of the Monte Carlo simulation for the two photon interaction performed by GVDM [25]. The details of LUND 5.3 and GVDM will be described in Section 3.3.1 and 3.4.2. The solid line show the sum of these Monte Carlo events. The good separation can be seen between the multi-hadronic events (right peak) and the two photon backgrounds (left peak), so that the $E_{vis} \geq E_{beam}$ cut removes the two photon backgrounds well.

The numbers of remaining events after the $E_{vis} \geq E_{beam}$ cut are 96 events at $\sqrt{s} = 50$ GeV, and 399 events at $\sqrt{s} = 52$ GeV. Hereafter, these events which pass these E_{LG}, $N_{goodtrack}$ and E_{vis} cuts are called the multi-hadronic events.

3.3. Detection Efficiency

3.3.1. Detection Efficiency

The detection efficiency of the VENUS detector for the multi-hadronic events was calculated by the Monte Carlo simulation. The simulation of multi-hadronic events is based on the LUND string fragmentation model developed by the LUND group. Their version 5.3 (LUND 5.3) was mainly used in this event generator [24].

The differential cross section of quark-antiquark pair production by the annihilation of electron-positron pair via one γ/Z^0 is expressed as follows:

$$\frac{d\sigma(q\bar{q})}{d\cos\theta} = \frac{\pi\alpha^2}{2s} \times Q_q^2$$
$$\times [(1+\cos^2\theta) - 2Q_q^{-1} Re(\chi(s)) \{(v_e v_q)(1+\cos^2\theta) + 2(a_e a_q)\cos\theta\}$$
$$+ Q_q^{-2} |\chi(s)|^2 \{(v_e^2+a_e^2)(v_q^2+a_q^2)(1+\cos^2\theta) + 8(v_e a_e v_q a_q)\cos\theta\}], \quad (3)$$

with

$$v_f = 2\tau_3 - 4Q_f \sin^2\theta_W, \quad a_f = 2\tau_3 (f = e, q), \quad (4)$$

$$\chi(s) = \frac{G_F}{8\sqrt{2}\pi\alpha} \times \frac{sM_Z^2}{s - M_Z^2 + iM_Z\Gamma_Z}, \quad (5)$$

where θ is the polar angle of the produced quark, τ_3 is the third component of weak iso spin. G_F is the Fermi coupling constant. M_Z is the mass of Z^0, and Γ_Z is the width of Z^0.

The initial radiation process in which the hard γ is emitted from the electron or

the positron before the annihilation, is taken into account. The probability of this γ emission is expressed to be $\delta_{hard}/(1+\delta)$, where δ_{hard} is the hard-γ component of the radiative correction $1+\delta$. (See Section 3.5 and Appendix B)

LUND 5.3 includes the gluon emission process from the primary quark or antiquark so as to reproduce the 3 jets structure of multi-hadronic events observed at PEP/PETRA [26]. The differential cross section of this process is written as follows:

$$\frac{1}{\sigma_0}\frac{d^2\sigma(q\bar{q}g)}{dx_1dx_2} = \frac{2\alpha_s}{3\pi}\frac{x_1^2+x_2^2}{(1-x_1)(1-x_2)}, \tag{6}$$

with

$$\sigma_0(e^+e^- \to q\bar{q}) = Q_q^2 \times 4\pi\alpha^2/3s, \tag{7}$$

$$x_i = 2E_i/\sqrt{s},$$

where x_1 and x_2 mean the fractional energies of quarks.

Then the quark and antiquark are hadronized according to the string fragmentation model. The energy fraction of produced quarks or antiquarks (x) is parameterized by the symmetric LUND fragmentation function as follows:

$$f(x) = \frac{(1-x)^a}{x}\exp\left(-\frac{bm_t^2}{x}\right), \tag{8}$$

where m_t is the transverse mass of each quark. a and b are the parameters. The transverse momentum p_t of hadrons are also parameterized as follows:

$$\frac{d\sigma}{dp_t^2} \propto \exp\left(-\frac{p_t^2}{\sigma_q^2}\right). \tag{9}$$

In addition to these parameters a, b, and σ_q, the parameter Y_{min} [24] called the minimum scaled invariant mass are used in this model. These parameter are set to the values which are determined by the PEP/PETRA experiments [27] as follows:

$$a = 1.0, \quad b = 0.63, \quad \sigma_q = 0.37, \quad \text{and} \quad Y_{min} = 0.02.$$

The detector responses for the generated events by the above Monte Carlo program were simulated by the program "VMONT" (Venus MONTe carlo simulator). This VMONT includes the calculations of the electromagnetic interactions between particles and detector material such as the ionization loss, γ conversion into e^+e^- pairs, and bremsstrahlung. The drift times along the track of each particle in CDC are calculated from the distance between the track and wire using the time-to-distance relation. These dift time are used in the tracking program which finds the tracks of the real events. The energy deposits in LG for electrons and gammas are also calculated by using the simulation program called EGS (version 4) developed at SLAC [28]. Nuclear interactions between particles of the strong interaction and materials are simulated by using the empirical formula developed by JADE group. The

informations on the responses are recorded by the VDS (Venus Data Structure) format which is used to analyse the real data, so that these Monte Carlo events can be analysed by the same programs such as the event selection program etc.

The simulated events reproduce well the distributions of real events as shown in Fig. 10, 11 and 12. Not only the distributions of various quantities which are used in the event selection, such as E_{LG}, $N_{goodtrack}$, P_{CDC} and E_{vis}, but also the distribution of $P_{charged}$ (momentum of charged particles), $E_{cluster}$ (cluster energy measured by the lead glass calorimeter), and the event shape parameters such as the thrust [29] and

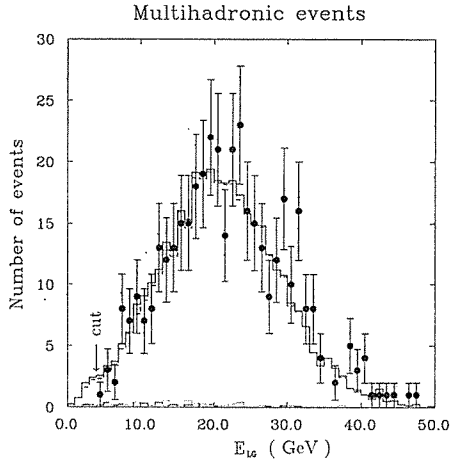

Fig. 10. E_{LG} distribution for the selected events (●). The solid line represents the result of the simulation including all the processes. The dashed line represents that for only the multi-hadronic events.

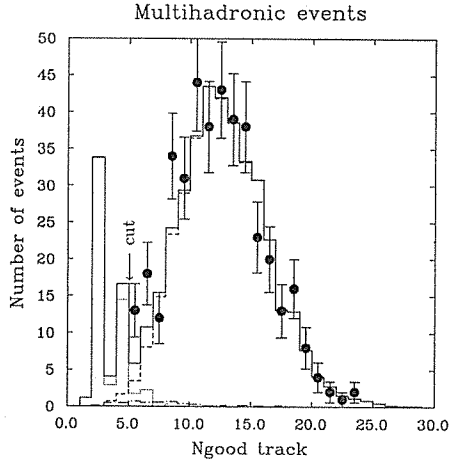

Fig. 11. $N_{goodtrack}$ distribution for the selected events (●). The solid line represents the result of the simulation including all the processes. The dashed line represents that for only the multi-hadronic events and the dotted line represents that for only tau pair events.

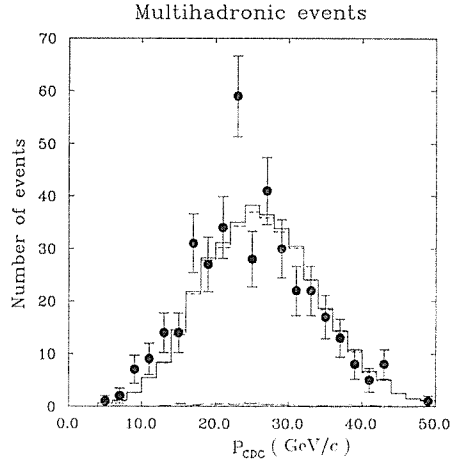

Fig. 12. P_{CDC} distribution for the selected events (●). The solid line represents the result of the simulation including all the processes. The dashed line represents that for only the multi-hadronic events.

sphericity [30] etc, well reproduce those for the real events within the statistical error.

The events which were generated by the above Monte Carlo simulation were analysed by the event selection program in the same manner for the real events. The efficiency was determined by dividing the number of selected events by the number of generated events. The efficiencies are calculated to be

$$\varepsilon = 69.2\% \pm 0.5\% \text{ at } \sqrt{s} = 50 \text{ GeV}, \quad \text{and}$$
$$\varepsilon = 68.3\% \pm 0.5\% \text{ at } \sqrt{s} = 52 \text{ GeV}.$$

The errors are due to the statistics of the Monte Carlo simulations.

3.3.2. Trigger Efficiency

The trigger efficiency for these selected multi-hadronic events were determined by checking the trigger pattern of the real multi-hadronic events at $\sqrt{s}=52$ GeV. First, all 399 multi-hadronic events were triggered by the condition of T1 in which the total energy deposit in LG is greater than 5 GeV (see Section 2.3.1). The lower limit corresponding to the 95% confidence level of this trigger efficiency is 99.2%. 396 multi-hadronic events among all 399 events were found to be triggered by the trigger condition of T3 in which two tracks recorded by CDC and TOF were collinear. The lower limit corresponding to the 95% confidence level of this trigger efficiency is 98.4%. Since these two trigger conditions are independent each other, the lower limit of the trigger efficiency for the selected multi-hadronic events can be written as

$$1-(1-0.992)\times(1-0.984) = 0.9999 .$$

This value shows that the trigger inefficiency is negligibly small.

3.3.3. Systematic Error of the Detection Efficiency

In order to estimate the systematic error of the detection efficiency, the detection efficiencies were calculated by generating the events with the different models such as LUND 6.3 and the Webber models. LUND 5.3 is based on the perturbative QCD and the string fragmentation, while LUND 6.3 [31] is based on the leading log parton shower scheme and the string fragmentation. The Webber model [32] is based on the leading log parton shower scheme and the cluster fragmentation. The difference among these detection efficiencies was found to be less than 1.2%.

The detection efficiencies were also calculated by changing the set values of the parameters such as a, b, σ_q and Y_{min} within the appropriate values. The difference of the detection efficiency by these changes were quadratically summed up to give one of systematic errors. The systematic error of this origin was found to be 4.5%.

Finally, the systematic error due to the selection criteria for the multi-hadronic events was estimated. The R ratios were calculated by changing the cut positions such as 3 GeV for the E_{LG} cut, 5 for the $N_{goodtrack}$ cut and E_{beam} for the E_{vis} cut by appropriate values. These variations of the R ratio were regarded as the systematic errors due to the selection criteria in our simulation. By adding these variations quadratically, the error amounted to 5.0%.

Then the systematic errors which depend on the models, parameters and selection

criteria were quadratically summed. The whole systematic error of the detection efficiency thus estimated amounts to 6.8%.

3.4. Background Estimation

In order to evaluate the total cross section of multi-hadron production via one γ/Z^0 annihilation, the background contamination must be carefully estimated. The background events due to the following origins were evaluated.

(1) beam-gas, beam-beam pipe interactions and cosmic rays
(2) two photon interaction
(3) tau pair production

3.4.1. Beam-Gas, Beam-Beam Pipe Interactions and Cosmic Rays

The tracks of the events from the beam-gas, beam-beam pipe interactions and cosmic rays do not come from the interaction point ($z=0$), because they are not produced by the e^+e^- interaction. These events are expected to be rejected by the $N_{goodtrack}\geq 5$ cut which requires 5 tracks from the interaction point as was discussed in Section 3.2. The following tests were made to estimate the contamination of these background events in our final multi-hadronic events. At first, about the same selection was applied by shifting the interaction point $z=0$ to the off centered position of $z=25$ cm. The number of the good tracks which come from around $z=25$ cm are counted. The conditions for the good tracks of this kind are expressed the same as the conditions for the multi-hadronic events. These are

$$N_{goodtrack}\geq 5 \text{ with } N_{hit-xy}\geq 8,\ N_{hit-rz}\geq 4,\ d_{r0}\leq 2 \text{ cm, and}$$
$$|d_{z0}-25|\leq 20 \text{ cm}.$$

Then, the $E_{LG}\geq 3$ GeV cut and the $E_{vis}\geq E_{beam}$ cut are also applied. Only one event remained after this test.

In addition to this test, the z-coordinate of the vertex averaged over all tracks in each multi-hadronic event was calculated. There is almost no tail beyond $|d_{z0}|\geq 20$ cm. Therefore, the contamination of these backgrounds is considered to be negligibly small.

3.4.2. Two Photon Interactions

The Monte Carlo simulation described in Section 3.2. ii) shows that the background events from the two photon interaction possess a small E_{vis} as shown in Fig. 9. These events are expected to be rejected by the $E_{vis}\geq E_{beam}$ cut. The contamination of the two photon interaction in the multi-hadronic events was estimated by a Monte Carlo simulation. In this simulation, the following two models were employed. The one is the generalized vector dominance model (GVDM [25]) and another is the quark parton model (QPM [33, 34]). In the GVDM process, it was assumed that a photon emitted from a positron (or electron) with a very small angle (quasi real photon) is converted to a vector meson (ρ, ω, ϕ, *etc*) and interacts with a electron (or positron). Subsequently a quark-antiquark pair is produced. These quarks are fragmented into two jets along to $+z$ and $-z$ direction, and then these

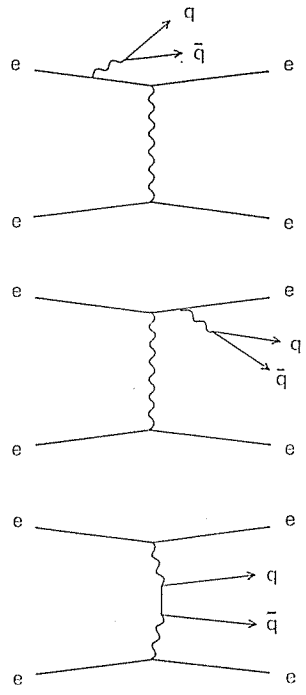

Fig. 13. Diagrams of the two photon quark parton model

jets are boosted to the laboratory frame. In the QPM process, a quark-antiquark pair is produced through the QED diagrams shown in Fig. 13. and then fragmented into two jets. Both in GVDM and QPM, the LUND string model was used in the fragmentation process. The production cross section of the QPM process can be exactly calculated by QED, however, the production cross section of the GVDM process can not be exactly calculated, so that the number of events which satisfy the $E_{LG} \geq 3$ GeV cut, $N_{goodtrack} \geq 5$ cut and $E_{vis} < E_{beam}$ cut (two photon cut) was normalized to the data.

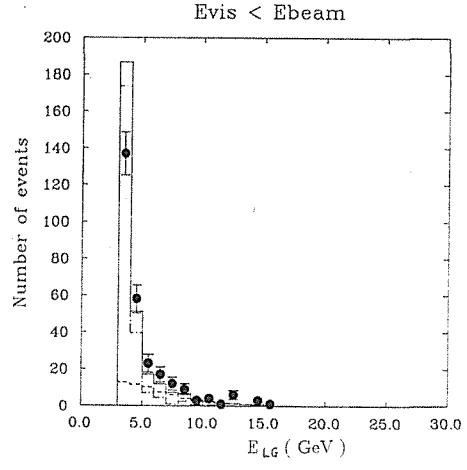

Fig. 14. E_{LG} distribution for the events with $E_{vis} \leq E_{beam}$ (●). The dashed, dot dashed and solid lines represent the results of the simulations for the multi-hadronic events, two photon events and the sum of them, respectively.

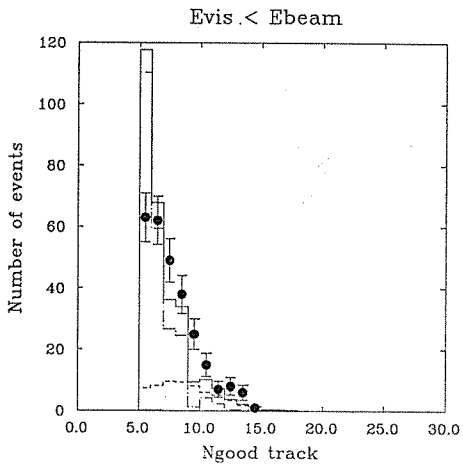

Fig. 15. $N_{goodtrack}$ distribution for the events with $E_{vis} \leq E_{beam}$ (●). The dashed, dot dashed and solid lines represent the results of the simulations for the multi-hadronic events, two photon events and the sum of them, respectively.

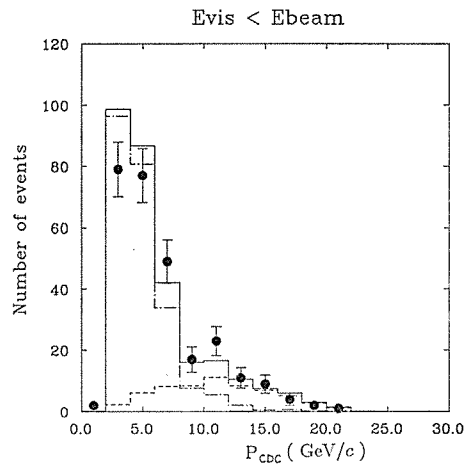

Fig. 16. P_{CDC} distribution for the events with $E_{vis} \leq E_{beam}$ (●). The dashed, dot dashed and solid lines represent the results of the simulations for the multi-hadronic events, two photon events and the sum of them, respectively.

In order to test how the GVDM and QPM processes can simulate the data, some of simulated distributions were compared with those for the selected events which satisfy above cuts. As shown in Fig. 14, 15, and 16, these Monte Carlo can well reproduce the data. With this Monte Carlo simulation, the background contamination after the multi-hadronic event selection can be estimated and found to be 0.2% for the GVDM process and 0.8% for the QPM process.

3.4.3. Tau Pair Production

The tau pair production was also simulated by a Monte Carlo simulation and is shown in Fig. 11. The result shows that these events have a small number of tracks and were well rejected by the $N_{goodtrack} \geq 5$ cut. The contamination of tau pair production for the multi-hadronic events was found to be 0.7%.

To check this contamination, the jet masses were also calculated for the selected multi-hadronic events. It was found that the jet masses of tau pair production are almost smaller than 3 GeV/c^2. A number of events in which both jet masses are smaller than 3 GeV/c^2 were found to be 7 for the selected multi-hadronic events, while the Monte Carlo simulations gave 6 events (3 from tau pair production and 3 from 5-flavor production of LUND version 5.3). This proves the validity of the Monte Carlo simulations.

Finally, the total fraction of the background amounts to 1.7% on an average.

3.5. Radiative Correction

In addition to the lowest order diagram, the higher order contribution to the multi-hadronic events via one γ/Z^0 annihilation is expected from the electro-weak

theory. Therefore, in order to obtain the cross section of multi-hadron production via one γ/Z^0 and to obtain the R ratio from our measurement, the observed cross section must be corrected by the facter so called "radiative correction" as $1/(1+\delta)$. This radiative correction $1+\delta$ is decomposed into four terms. These are

$$1+\delta = 1+\delta_{vac}+\delta_{ver}+\delta_s+\delta_h\,, \tag{10}$$

with δ_{vac}: vacuum polarization of leptons and hadrons
δ_{ver}: vertex correction
δ_s : soft initial state radiation
δ_h : hard initial state radiation.

The soft radiation means $k_\gamma \leq k_{min}$ and the hard radiation means $k_{min} < k_\gamma < k_{max}$ ($k_\gamma = E_\gamma/E_{beam}$). In this analysis, k_{min} and k_{max} were set to be 0.01 and 0.99, respectively.

δ was calculated by the method developed by Berends, Kleiss and Jadach [35]. In this calculation, the infra-red divergences of δ_{ver} and δ_s are cancelled each other, so that the exact values can be calculated. The leptonic part of vacuum polarization can also be calculated exactly. The exact expressions are given in Appendix B. For the calculation of the hadronic part of vacuum polarization and hard initial radiation, the cross section $\sigma(s')$ for multi-hadronic events at lower energies is needed. The value of $\sigma(s')$ was calculated by using the empirical formula developed by the LUND group.

Finally, δ was calculated by using the parameters $\sin^2\theta_W = 0.225$, $M_Z = 92.6$ [36] and $\Lambda_{\overline{MS}} = 800$ MeV [37] and amounted to

$$1+\delta = 1.32 \text{ at } \sqrt{s} = 50 \text{ GeV}\,, \quad \text{and}$$
$$1+\delta = 1.31 \text{ at } \sqrt{s} = 52 \text{ GeV}\,.$$

The systematic error of the radiative correction $1+\delta$ due to the uncertainty of $\sigma(s')$ was estimated to be about 1% by changing $\sigma(s')$ by 10%. The systematic error due to the parameters such as $\sin^2\theta_W$, M_Z and $\Lambda_{\overline{MS}}$ was also estimated by changing them appropriately and amounts to about 1%. It was pointed out that δ_{ver} can be varied by changing the renormalization scheme of Berends et al. The systematic error due to this origin was estimated to be about 1.5%. Adding these errors quadratically, the systematic error of radiative correction $1+\delta$ was estimated to be 2%.

3.6. Integrated Luminosity

The luminosity was evaluated from the data of the large angle and small angle Bhabha scattering measured by LG–CDC and LM (luminosity monitor), respectively. A number of the small angle events was far larger than that of the large angle scattering because of the characteristic of the angular dependence. The integrated luminosities calculated from both events agree with each other, however, the subtraction of background and the accuracy of positioning caused a large systematic error for the small angle events. Therefore, in this analysis, the integrated luminosity evaluated from the large angle scattering was used to evaluate the cross section and the R ratio in the same way as done at PEP/PETRA, because of the small systematic error.

The Bhabha scattering events were selected as follows [38]:

i) Numbers of high energy electrons (positrons) ≥ 2
where the high energy electrons (positrons) were required to have the "good track" within the angular range of $|\cos\theta| \leq 7.43$ and to deposit the energies greater than $E_{beam}/3$ in LG.

ii) $\theta_{acoll}(e^+-e^-) \leq 10°$
where θ_{acoll} is the acollinearity angle between the tracks of the high energy electron and positron.

iii) Number of good tracks with $P_{xy} \geq 1.0$ GeV is at least 2 and at most 4.

Finally, 306 and 1191 events remained after these cuts at $\sqrt{s}=50$ and 52 GeV, respectively. The integrated luminosity was evaluated by the following equation.

$$L = \frac{N_B(1+C)}{\varepsilon_B(1+\sigma_B)\sigma_B}, \tag{11}$$

with N_B: number of the selected Bhabha events by the previous event selection
ε_B : detection efficiency for the Bhabha events, which was estimated by the Monte Carlo simulation developed by Tobimatsu et al [39].
σ_B : cross section of the Bhabha scattering, which was calculated by Tobimatsu et al [39].
δ_B : radiative correction which was also calculated by Tobimatsu et al [39].
C : sum of the various correction factors.

C can be decomposed as follows:

$$C = C_{bg}+C_{ee\gamma}+C_{Brems}+C_{dead}+C_{miss}$$

with

C_{bg} $=-0.5\%$: correction factor due to the background subtraction
$C_{ee\gamma}$ $=+1.3\%$: correction factor which comes from the fact that the low energy ($E \leq E_{beam}/3$) electron (positron) is mis-identified as the high energy ($E \geq E_{beam}/3$) electron (positron) due to the radiative γ in the $e^+e^- \to e^+e^-\gamma$ event.
C_{Brems} $=-1.5\%$: correction factor which comes from the fact that the high energy electron (positron) losses its energy by radiating the bremsstrahlung in the detector and is mis-identified as the low energy electron (positron).
C_{dead} $=+0.7\%$: correction factor due to dead PMT's of LG.
C_{miss} $=+0.4\%$: correction factor due to the inefficiency of tracking.

The values of the integrated luminosity thus evaluated are

$$L = 0.695 \pm 0.040 \pm 0.018 \text{ pb}^{-1} \quad \text{at } \sqrt{s} = 50 \text{ GeV}, \quad \text{and}$$
$$L = 2.912 \pm 0.084 \pm 0.075 \text{ pb}^{-1} \quad \text{at } \sqrt{s} = 52 \text{ GeV},$$

where the first and second errors are statistical and systematic ones, respectively.

The systematic error of the integrated luminosity amounts to 2.6% by summing up the errors from the correction factor (0.4%) and the detection efficiency (2.5%).

4. RESULTS AND DISCUSSION

4.1. Total Cross Section of Multi-hadron Production and the R ratio

Experimentally, the total cross section of multi-hadron production was evaluated from the measured events by using the following expression:

$$\sigma(e^+e^- \to (\gamma/Z^0)^* \to \text{hadrons}) = \frac{N_h(1-\sum f_{bg})}{\varepsilon(1+\delta)L}, \tag{12}$$

with N_h : number of observed multi-hadronic events
f_{bg} : fraction of background
ε : detection efficiency
$1+\delta$: radiative correction
L : integrated luminosity (nb^{-1}).

Using the values given in the previous sections, the cross sections were evaluated to be as follows:

$$\sigma_m = 148 \pm 17 \pm 11 \text{ pb at } \sqrt{s} = 50 \text{ GeV}, \quad \text{and}$$
$$\sigma_m = 150 \pm 9 \pm 11 \text{ pb at } \sqrt{s} = 52 \text{ GeV},$$

where the first error is the statistical error and estimated as $\sigma \times \sqrt{1/N_h + 1/N_B}$. The second error is the sum of the systematic errors of 6.5%, 2.0%, and 2.6% due to the efficiency and background fraction, radiative correction, and integrated luminosity, respectively. The sum of these systematic errors amounts to 7.3%.

Then the R ratio is evaluated from these cross sections of the multi-hadron production, by using the Eq. (1) and the following value,

$$\sigma_{point} = \frac{4\pi\alpha^2}{3s} = \frac{86.9}{s(\text{GeV}^2)} \text{ (nb)}. \tag{13}$$

The measured R ratio are

$$R_m = 4.27 \pm 0.50 \pm 0.31 \text{ at } \sqrt{s} = 50 \text{ GeV} \quad \text{and}$$
$$R_m = 4.68 \pm 0.27 \pm 0.34 \text{ at } \sqrt{s} = 52 \text{ GeV}.$$

These values are shown in Fig. 17 together with the data at PEP/PETRA [40] and with the theoretical predictions with the five quarks. The R ratio including not only the lowest order QED diagram but also the higher order QCD contribution and the lowest order electro-weak contribution can be expressed as follows:

$$\begin{aligned} R &= \sum_q 3Q_q^2 \times (1+C_{QCD}) \times (1+C_{Weak}) \\ &= \sum_q 3Q_q^2 \times \{1 + C_1 \alpha_s(s)/\pi + C_2(\alpha_s(s)/\pi)^2\} \\ &\quad \times [1 - 2Q_q^{-1} Re(\chi(s))\, v_e v_q + Q_q^{-2} |\chi(s)|^2 \{(v_e^2+a_e^2)(v_q^2+a_q^2)\}], \end{aligned} \tag{14}$$

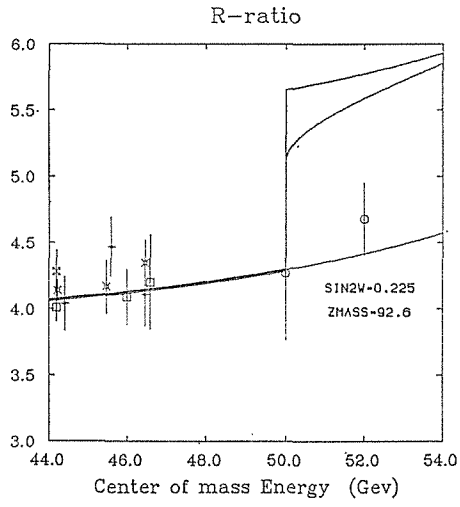

Fig. 17. R ratio as a function of the CM energy

where $\{1+C_1\,\alpha_s(s)/\pi+C_2(\alpha_s(s)/\pi)^2\}$ represents the correction factor by QCD. The coefficient $C_1=1$ and $C_2=1.986-0.115\,N_q$ in the $\overline{MS}$ scheme [41]. N_q is the number of existing quarks ($=5$). $\alpha_s(s)$ is given by

$$\alpha_s(s)=\frac{12\pi}{(33-2N_q)\log(s/\Lambda^2_{\overline{MS}})+6\dfrac{153-19\,N_q}{33-2\,N_q}\log(\log(s/\Lambda^2_{\overline{MS}}))}\,, \qquad (15)$$

where $\Lambda_{\overline{MS}}$ is the QCD scale parameter in the $\overline{MS}$ scheme [42]. v_e, v_q, a_e, a_q and $\chi(s)$ are given by the Eq. (4) and Eq. (5) in Section 3.3.1.

Using the parameters $\sin^2\theta_W=0.225$, $M_Z=92.6$ [36] and $\Lambda_{\overline{MS}}=800$ MeV [37], the theoretical values of the R ratio with known five quarks such as u, d, s, c and b are evaluated to be

$$R_{5q}=4.31 \text{ at } \sqrt{s}=50 \text{ GeV}\,, \quad \text{and}$$
$$R_{5q}=4.43 \text{ at } \sqrt{s}=52 \text{ GeV}\,.$$

The measured R ratios are consistent with the theoretical prediction with the production of known five quarks.

4.2. Top Quark

The existence of the open top quark production was tested from our measurement. The detection efficiency and the radiative correction for the top quark production depend on the mass of the top quark, and are different from those for the five quark production. However, the product $\varepsilon(1+\delta)$ is not so different from that for the five quark production. Their values are evaluated by a Monte Carlo simulation and are seen in Table 2. Considering the difference of $\varepsilon(1+\delta)$ between the top quark production and the known five quark production, the R ratio including the open top

quark production is expected to be measured as

$$R_{6q} = 5.49 \text{ at } \sqrt{s} = 50 \text{ GeV} \quad \text{for} \quad m_{top} = 24 \text{ GeV}/c^2, \quad \text{and}$$
$$R_{6q} = 5.61 \text{ at } \sqrt{s} = 52 \text{ GeV} \quad \text{for} \quad m_{top} = 25 \text{ GeV}/c^2.$$

In this calculation, the threshold effect is neglected. The QCD effect and the axial coupling part of the neutral current are also neglected for the top quark.
The upper limits of $\delta R = R_m - R_{5q}$ with the confidence level of 95% can be calculated by the expression of

$$\delta_{95\%} R \equiv R_m + 1.96 \sqrt{\Delta R^2_{stat} + \Delta R^2_{syst}} - R_{5q},$$

and were found to be

$$\delta_{95\%} R = 1.19 \text{ at } \sqrt{s} = 50 \text{ GeV}, \quad \text{and}$$
$$\delta_{95\%} R = 1.14 \text{ at } \sqrt{s} = 52 \text{ GeV}.$$

In terms of the cross sections, the upper limits of $\delta\sigma = \sigma_m - \sigma_{5q}$ with the confidence level of 95% were found to be

$$\delta_{95\%} \sigma = 41 \text{ pb at } \sqrt{s} = 50 \text{ GeV}, \quad \text{and}$$
$$\delta_{95\%} \sigma = 37 \text{ pb at } \sqrt{s} = 52 \text{ GeV}.$$

The difference between the theoretical R ratio with and without the top quark ($\delta_{top} R \equiv R_{6q} - R_{5q}$) are

$$\delta_{top} R = 1.18 \text{ at } \sqrt{s} = 50 \text{ GeV} \quad \text{and} \quad m_{top} = 24 \text{ GeV}/c^2, \quad \text{and}$$
$$\delta_{top} R = 1.18 \text{ at } \sqrt{s} = 52 \text{ GeV} \quad \text{and} \quad m_{top} = 25 \text{ GeV}/c^2.$$

The difference between the predicted cross sections of multi-hadron production with and without the top quark ($\delta_{top} \sigma \equiv \sigma_{6q} - \sigma_{5q}$) are

$$\delta_{top} \sigma = 41 \text{ pb at } \sqrt{s} = 50 \text{ GeV} \quad \text{and} \quad m_{top} = 24 \text{ GeV}/c^2, \quad \text{and}$$
$$\delta_{top} \sigma = 38 \text{ pb at } \sqrt{s} = 52 \text{ GeV} \quad \text{and} \quad m_{top} = 25 \text{ GeV}/c^2.$$

The values of $\delta_{top} R$ and $\delta_{top} \sigma$ are almost equal to those of $\delta_{95\%} R$ and $\delta_{95\%} \sigma$. These facts give us the conclusion that the open top quark production up to $m_{top} = 25 \text{ GeV}/c^2$ is rejected with the confidence level of 95%.

Table 2 Mass dependence of the efficiency and radiative correction for the top quark production

$E_{beam} - m_{top}$	$1+\delta$	ε	$\varepsilon(1+\delta)$
2.0 GeV	0.95	0.898	0.853
1.0 GeV	0.88	0.906	0.797
0.5 GeV	0.82	0.911	0.742

4.3. Electro-Weak Theory

The R ratio given by Eq. (14) depends on the parameter of the Weinberg angle $\sin^2\theta_W$ through v_e and v_q which are given in Eq. (4). M_Z is included in $\chi(s)$ given by Eq. (5) and can be expressed in terms of $\sin^2\theta_W$ as follows:

$$M_Z = \sqrt{\frac{\pi\alpha}{\sqrt{2}\,G_F}} \times \sqrt{\frac{1}{\sin^2\theta_W(1-\sin^2\theta_W)\,(1-\delta r_{mZ})}}\ , \tag{16}$$

where δr_{mZ} [43] is the radiative correction of mass of Z^0 and estimated to be 0.069 ± 0.020 [44]. In the energy region of TRISTAN, the $\sin^2\theta_W$ dependence of the R ratio is greater than in the lower energy region as PEP/PETRA. Therefore, $\sin^2\theta_W$ can be determined from the measured R ratio. Using the parameter $N_q=5$, $\delta r_{mZ}=0.069$ and $\Lambda_{\overline{MS}}=800$ MeV, the value of $\sin^2\theta_W$ was evaluated from the measured R ratios and is

$$\sin^2\theta_W = 0.26\pm0.04\pm0.06\ .$$

The corresponding M_Z is

$$M_Z = 88\pm5\pm8\ \mathrm{GeV}/c^2\ ,$$

where the first error comes from the statistical error of the R ratio and the second error comes from the systematic error of the R ratio and the error of δr_{mZ}. ($\chi^2/l=0.163$)

5. SUMMARY

The total cross sections of multi-hadron production for the e^+e^- annihilation have been measured with an accuracy of 7% at the CM energy of 50 and 52 GeV with the VENUS detector in TRISTAN. The results of the R ratio are

$$R = 4.27\pm0.50\pm0.31 \text{ at } \sqrt{s} = 50 \text{ GeV} \quad \text{and}$$
$$R = 4.68\pm0.27\pm0.34 \text{ at } \sqrt{s} = 52 \text{ GeV}\ .$$

The present results show the increase of the R ratio above $\sqrt{s}=40$ GeV, which is expected from the electro-weak interaction through the Z^0 production. These values are consistent with the prediction from the standard model with the production of known five quarks u, d, s, c and b. However, the expected R ratios including the t quark are 5.49 at $\sqrt{s}=50$ GeV and 5.61 at $\sqrt{s}=52$ GeV and are much lager than the observed values. These results reject the production of the open top quark at $\sqrt{s}=52$ GeV with the confidence level of 95%.

The Weinberg angle $\sin^2\theta_W$ was also determined from the R ratios by using the relation based on the standard $SU(3)_{color}\otimes SU(2)_L\otimes U(1)$ model and found to be $\sin^2\theta_W = 0.26\pm0.04\pm0.06$.

ACKNOWLEDGEMENT

First I wish to express my great appreciation to professor K. Miyake for his continuous guidance and advices throughout this study. I acknowledge to Dr. N.

Tamura, Dr. Y. Henmi, Mr. K. Kubo, Mr. H. Kurashige and other member of Kyoto University for their effort in construction of the TOF counter in which I was involved. I am deeply indebted to the members of VENUS group for their continuous work in construction and successful operation of our VENUS detector. I also thank Dr. J. Kanzaki for his continuous support and valuable advices in the analysis.

APPENDIX

A. TOF COUNTER SYSTEM

A.1. Design

The TOF counter system was required to give a trigger signal for the charged particles from the e^+e^- interaction, and it was also required to identify the particles such as π, K, and p in the multi-hadronic events. In order to provide a large solid angle and a long flight path, it was installed on the inner wall of the superconducting magnet whose diameter and length are 340 cm and 564 cm, respectively. The TOF counter system is segmented into ninety six scintillation counters of 10.8 cm wide, 4.2 cm thick, and 466 cm long as shown in Fig. 18, and is formed into a barrel. The size of TOF counter system turned out to be the world largest size among the TOF counters for the collider detectors. Taking into account the cost and the easiness of installation, this number of segments was determined by the Monte Carlo simulation, so that the number of charged particles which hit one counter is almost one. Fig. 19 shows the number of charged particles which hits one counter for the measured hadronic events at $\sqrt{s}=52$ GeV. The rate of a single hit was found to be about 88%.

A.2. Scintillator and Phototubes

The time resolution of the TOF counter system is required to be less than 200

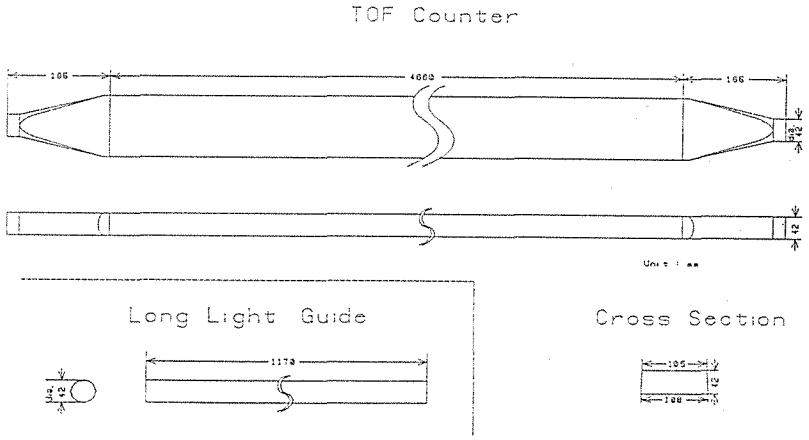

Fig. 18. Dimensions of the TOF counter

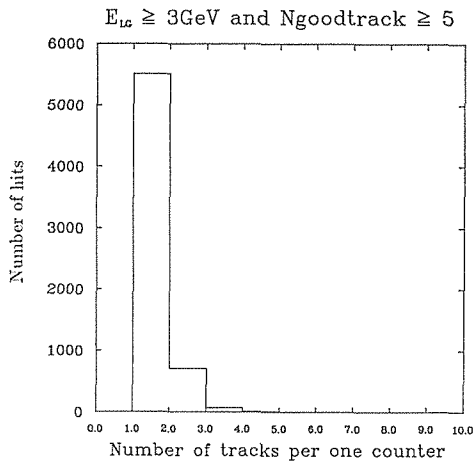

Fig. 19. Number of charged particles which hits one counter for the hadronic event

psec for identifying π/K and K/p whose momentum is less than 1 GeV/c. In order to realize this good resolution with our large TOF counter system, the scintillator is required to emit a large number of photons and has a long attenuation length. Four kinds of scintillators were tested. These are NE110 of Nuclear Enterprise Corp., SCSN23 and SCSN38 of Kyowa Gas Chemical, and BC408 of Bicron Corp.. The size of the test samples was 10 cm wide, 5 cm (4 cm) thick, and 400 cm long. The samples were viewed by a pair of phototubes on both ends through a long light guide. Muons which penetrated through the beam dump of KEK 12 GeV Proton Synchrotron were used to measure the attenuation length of light and the time resolution of these scintillators. The results are shown in Fig. 20. Comparing the time resolutions after the pulse height correction, it was found that NE110 and SCSN23 satisfied our requirements. Finally, we chose the SCSN23 scintillator of Kyowa Gas Chemical with 4.2 cm thickness for our TOF counters taking into account the cost and resistivity against the mechanical stress. The phototubes of H1949 manufactured by Hamamatsu Photonics which were newly designed for the fast timing purpose were chosen because of their small spread of the transit time.

A.3. Test and Calibration

The attenuation length and the time resolution of each counters were measured by using cosmic rays before the installation into the VENUS detector. The attenuation length distributed between 2.5 m and 3.3 m and was 2.9 m on an average. A small decrease in the attenuation length was observed during these measurements. We suspect that the main origin is a slow degradation of the polished surface. Fig. 21 shows the distribution of the time resolution measured with the cosmic rays which hit the center of counter. The average time resolution was found to be 175 psec after the pulse height correction.

In order to maintain the TOF counter with a good time resolution throughout the long period of the experiment, we provided a calibration system. Fig. 22 shows

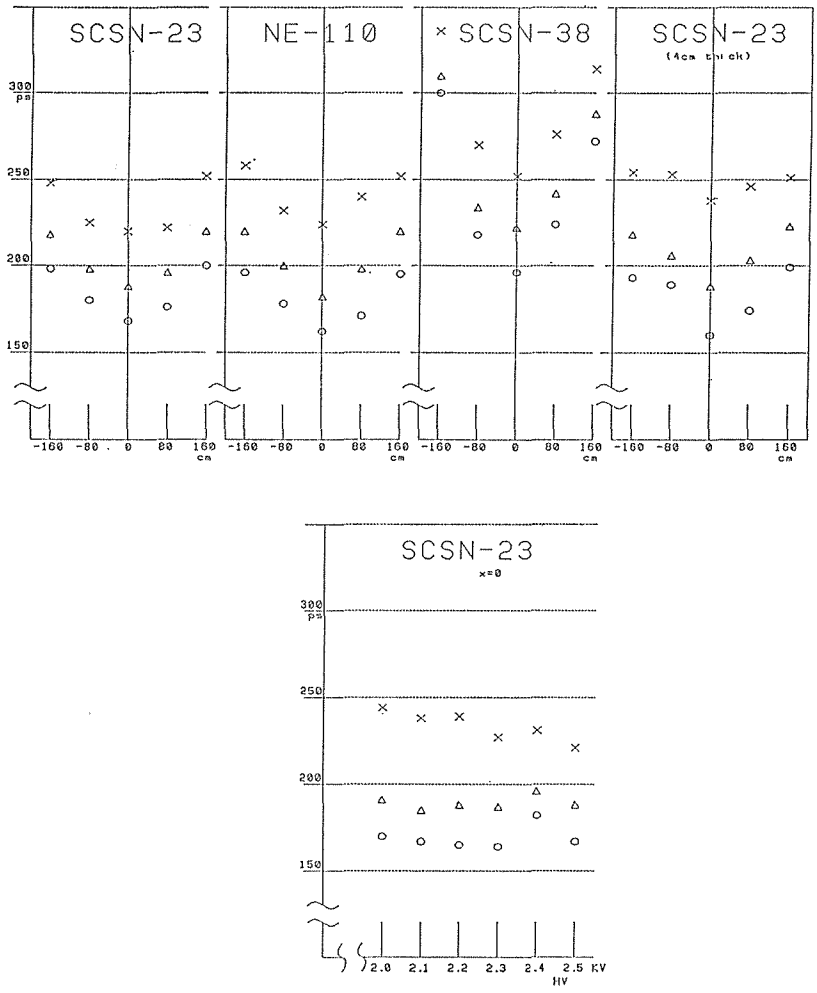

Fig. 20. Dependence of the time resolution (a) on incident position and (b) on HV of phototubes.
×: Time resolution before the pulse height correction.
△: Time resolution after the correction.
○: Intrinsic time resolution.

our calibration system. The visible light pulse which is converted in Dye laser from ultraviolet lights of a Nitrogen laser has a wavelength of 570 nm and a pulse width of 100 psec. These light pulses are fed to the light guide of the TOF counter through optical quartz fibers whose diameter is 200 μm. By measuring the time difference between the signal of vacuum photodiode near the Dye laser and the signal of the phototube in the TOF counter, the intrinsic time resolution of our TOF counter system was measured to be about 75 psec.

A.4. Performances

Our TOF counter system has been operated since November 1986. In order

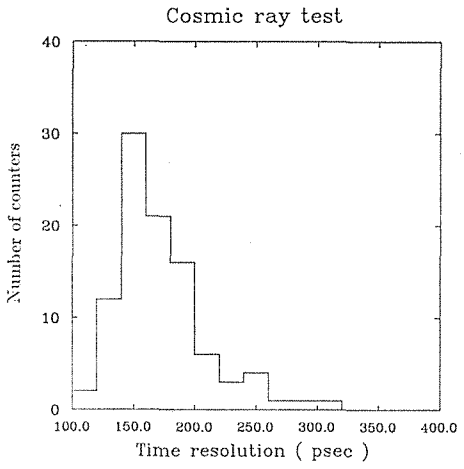

Fig. 21. Time resolution of the TOF counter

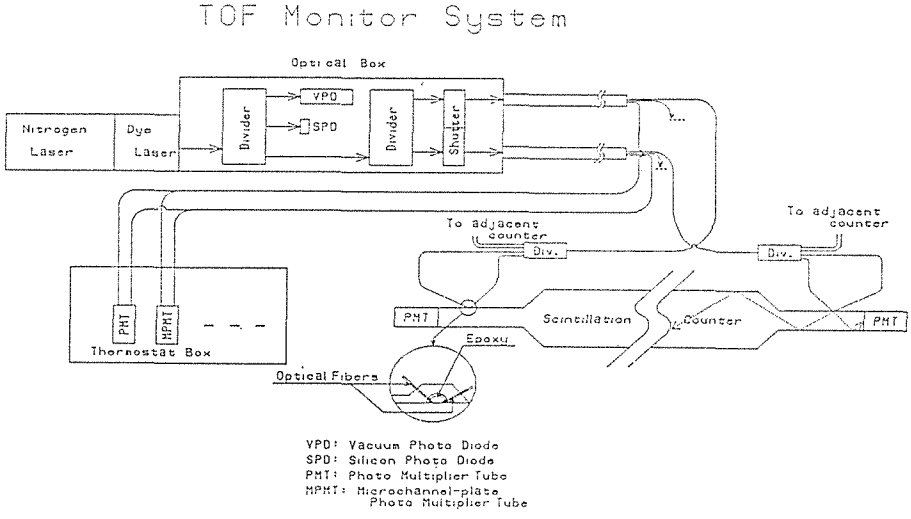

Fig. 22. Calibration system of the TOF counter

to trigger the charged particles of e^+e^- interactions with a small contamination of cosmic rays, signals of the TOF counter generated within 150 nsec from the beam crossing time were used for collinear two track trigger associated with the signals of track finder of CDC. The flight time of particles can be evaluated by subtracting the propagation time in scintillator and electronics from the measured time difference between the beam crossing signal and the signal from the TOF counter. This propagation time was evaluated by using the high momentum particles of higher than 2 GeV/c in the hadronic events because the velocity of these particles are very close to the light velocity. Using the propagation time evaluated by the above method, the time resolution of 410 psec was achieved at the present stage. Fig. 23 shows the time resolution of the TOF counter which is determined by calculating the time difference between the measured flight time and the expected flight time for the tracks

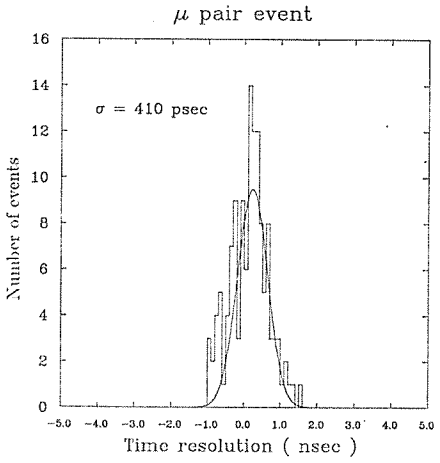

Fig. 23. Time resolution of the TOF counter which is determined by calculating the time difference between the measured flight time and the espected flight time for the tracks of μ pair events.

of μ pair events.

B. RADIATIVE CORRECTION

As mentioned in Section 3.5, the radiative correction factor of the electro-weak theory $1+\delta$ was calculated by the method of Berends, Kleiss and Jadach [35].

The part of radiative corrections without initial radiation can be calculated as follows (divergent terms are neglected):

$$\delta_{ver}+\delta_{vac} = \frac{\alpha}{\pi}\times\left[\frac{3}{2}\left(\ln\frac{s}{m_e^2}-1\right)-\frac{1}{2}+\frac{2}{3}\pi^2\right.$$
$$+\frac{2R_{QQ}+\dfrac{\zeta}{B(0)}R_{QV}}{R_{SUM}}\times\left\{\frac{2}{3}\sum_{f=l}\left(\ln\frac{s}{m_f^2}-\frac{5}{3}\right)+\delta_{VP-h}\right\}$$
$$\left.+\frac{\gamma}{B(0)}\frac{R_{QV}}{R_{SUM}}\times\frac{\pi}{3}\sum_{f=l,\tau}Q_f^2\right], \qquad (17)$$

with

$$\zeta = 1-\frac{M_Z^2}{s}, \quad \gamma = \frac{M_Z\Gamma_Z}{s}, \quad B(k) = (\zeta-k)^2+\gamma^2,$$

and

$$R_{QQ} = 3\sum_{f=q}Q_f^2,$$

$$R_{QV} = -\frac{6v_e}{4\sin^2 2\theta_W}\sum_{f=q}Q_f v_f,$$

$$R_{VA} = \frac{3(v_e^2+a_e^2)}{(4\sin^2 2\theta_W)^2}\sum_{f=q}(v_f^2+a_f^2),$$

$$R_{SUM} = R_{QQ} + \frac{\zeta}{B(0)} R_{QV} + \frac{1}{B(0)} R_{VA} .$$

The term of δ_{VP-h} can be written by the empirical expression of hadronic vacuum polarization developed by the LUND group as follows:

$$\begin{aligned}\delta_{VP-h} &= \frac{s}{2\pi^2 \alpha} \int_{4m_\pi^2}^{\infty} \frac{\sigma(s')}{s-s'} \mathrm{d}s' \\ &\cong \frac{\alpha}{\pi} \times 3.052 \ln \frac{s}{0.932} .\end{aligned} \tag{18}$$

The soft initial radiation part can be calculated by the following expression.

$$\begin{aligned}\delta_s = & \frac{\alpha}{\pi}\left(\ln\frac{s}{m_e^2} - 1\right) \\ & \times \Bigg[2 \ln k_{min} - \frac{R_{QQ}}{R_{SUM}} \ln(1-k_{min}) - \frac{R_{QQ}+R_{QV}+R_{VA}}{R_{SUM}} k_{min} \\ & + \frac{R_{QV}\left(1-\frac{\zeta}{2}-\frac{\zeta}{B(0)}\right) + R_{VA}\left(\frac{3}{2}-\zeta-\frac{1}{B(0)}\right)}{R_{SUM}} \ln\frac{B(k_{min})}{B(0)} \\ & + \frac{R_{QV}\gamma^2\left(1-\frac{2}{B(0)}\right) + R_{VA}\left(\frac{2\zeta}{B(0)}+\gamma^2-4-3\zeta-\zeta^2\right)}{\gamma R_{SUM}} \\ & \times \left\{ \arctan\left(\frac{k_{min}-\zeta}{\gamma}\right) - \arctan\left(\frac{-\zeta}{\gamma}\right) \right\} \Bigg] .\end{aligned} \tag{19}$$

If we assume

$$\sigma(s') = \sum_q 3Q_q^2 \times \frac{4\pi\alpha^2}{3s'} ,$$

where s' is the energy of the center of mass system after the initial radiation, the hard initial radiation part can be calculated by the following expression,

$$\begin{aligned}\delta_h = & \frac{\alpha}{\pi}\left(\ln\frac{s}{m_e^2} - 1\right) \times \Bigg[\frac{R_{QQ}}{R_{SUM}} \times \int_{x_{min}}^{x_{max}} \mathrm{d}x \left\{ \frac{1}{x}\left(\frac{1}{1-x}+1-x\right) f(x) \right\} \\ & + \frac{R_{QV}}{R_{SUM}} \frac{\zeta}{B(0)} \times \int_{x_{min}}^{x_{max}} \mathrm{d}x \left\{ \frac{1}{x}\left(1+(1-x)^2\right)(\zeta-x) f(x) \right\} \\ & + \frac{R_{VA}}{R_{SUM}} \frac{1}{B(0)} \times \int_{x_{min}}^{x_{max}} \mathrm{d}x \left\{ \frac{1}{x}\left(1+(1-x)^2\right)(1-x) \frac{1}{B(x)} f(x) \right\} \Bigg] ,\end{aligned} \tag{20}$$

with

$$\begin{aligned} & x_{min} = k_{min},\ x_{max} = max(k_{max},\ 1-m_q/E_{beam}) , \\ & f(x) = \sqrt{\frac{1-\beta/(1-x)}{1-\beta}} \frac{2+\beta/(1-x)}{2+\beta} ,\end{aligned}$$

and

$$\beta = \sqrt{1-(m_q/E_{beam})^2} \ .$$

References

[1] S. L. Glashow, Nucl. Phys. **22** (1961) 579;
S. Weinberg, Phys. Rev. Lett. **19** (1967) 1264;
A. Salam, *Proc. of the Eighth Nobel Symposium, May* 1968.

[2] H. Fritzsch et al., Phys. Lett. **B47** (1973) 365;
D. J. Gross and F. Wilczek, Phys. Rev. **D8** (1973) 3633;
H. D. Politzer, Phys. Rev. Lett. **31** (1973) 31.

[3] J. E. Augustin et al., Phys. Rev. Lett. **33** (1974) 1406.

[4] J. J. Aubert et al., Phys. Rev. Lett. **33** (1974) 1404.

[5] S. L. Glashow, J. Iliopoulos and L. Maiani. Phys. Rev. **D2** (1970) 1285.

[6] M. L. Perl et al., Phys. Rev. Lett. **35** (1975) 1489.

[7] S. Herb et al., Phys. Rev. Lett. **39** (1977) 252.

[8] G. Flügge, *Proc. of the 19th Int. Conf. on High Energy Physics*, 1978, *Tokyo.*

[9] For example, S. Komamiya, *Proc. of the* 1985 *Int. Symp. on Lepton and Photon Interactions at High Energies, August* 19–24, 1985, *Kyoto.*

[10] TRISTAN Project Group, TRISTAN ELECTRON-POSITRON COLLIDING PROJECT, KEK report 86–14 (1986).

[11] VENUS Collab., J. Iwahori et al., VENUS proposal, KEK report (1983).

[12] T. K. Ohska, et al., IEEE Trans. on Nucl. Sci. **33**, (1986) 98.;
TKO Specification, KEK Report 85–10 (1985).

[13] Y. Yamada, et al., KUNS 853, 1987, Kyoto Univ.;
K. Kubo, Memoirs of the Facglty of Science, Kyoto University, Series of Physics, Astrophysics, Geophysics and Chemistry, Vol, XXXVII No. 3, 125 (1989)

[14] R. Arai, et al., Nucl. Instrum. Methods. **217** (1983) 181.

[15] IEEE Standard FASTBUS Modular High-Speed Data Acquisition and Control System, ANSI/ IEEE Std 960–1986.

[16] Y. Hemmi et al., Japan J. Appl. Phys. **26** (1987) 982.

[17] R. Arai et al., Nucl. Instrum. Methods. **A254** (1987) 317.

[18] K. Ogawa et al., Nucl. Instrum. Methods. **A243** (1986) 58;
T. Sumiyoshi et al., KEK preprint 87–120 (1987), submitted to Nucl. Instrum. and Methods.

[19] Y. Asano et al., Nucl. Instrum. and Methods. **A259** (1987) 430.

[20] Y. Chiba et al., to be published.

[21] T. Ohsugi, et al., to be published in Nucl. Instrum. and Methods.

[22] Y. Yasu, et al., IEEE Trans. on Nucl. Sci. **31**(1984) 197.

[23] Y. Nakagawa, T. Hirose and J. Kanzaki, KEK preprint 85–67 (1985), submitted to Japan J. Appl. Phys..

[24] B. Andersson, G. Gustafson, G. Ingelman and T. Sjöstrand, Phys. Rep. **97** (1983) 31.

[25] For example, V. M. Bundev et al., Phys. Rep. **15C** (1975) 182;
PLUTO Collab., C. Barger et al., Phys. Lett. **B81** (1979) 410 and Phys. Lett. **B99** (1981) 287.

[26] For example, P. Söding, *Proc. of EPS Int. Conf. on High Energy Physics, July*, 1979, *Geneva.*

[27] CELLO Collab., H.-J. Behrend et al., Phys. Lett. **B138** (1984) 311;
TPC/Two-Gamma Collab., H. Aihara et al., Z. Phys. **C28** (1985) 2724;
MAC Collab., E. Fernandez et al., Phys. Rev. **D31** (1985) 2724;
JADE Collab., W. Bartel et al., Z. Phys. **C33** (1986) 23.

[28] R. L. Fold and W. R. Nelson, Preprint SLAC-210, UC-32, 1978

[29] E. Farhi, Phys. Rev. Lett. **39** (1977) 1587.

[30] J. D. Bjorken and S. J. Brodsky, Phys. Rev. **D1** (1970) 1416;
G. Hanson et al., Phys. Rev. Lett. **35** (1975) 1609.

[31] T. Sjöstrand, Comput. Phys. Commun., **39** (1986) 347;
T. Sjöstrand and M. Bengtsson, Comput. Phys. Commun., **43** (1987) 367.
[32] B. R. Webber, Nucl. Phys. **B238** (1984) 492.
[33] For example, S. J. Brodsky, F. E. Close and J. F. Gunion, Phys. Rev. **D6** (1972) 177
[34] S. Kawabata, Comput. Phys. Commun., **41** (1986) 127.
[35] F. Berends, R. Kleiss and S. Jadach, Nucl. Phys. **B202** (1982) 63;
Comput. Phys. Commun. **29** (1983) 185.
[36] Particle Data Group, Phys. Lett. **B170** (1986) 1
[37] J. Jersák, E. Laermann and P. M. Zerwas, Phys. Lett. **B98** (1981) 363 and Phys. Rev. **D25** (1982) 1218.
[38] VENUS Collab., K. Abe et al., J. Phys. Soc. Jpn. **11** (1987) 3767.
[39] K. Tobimatsu and Y. Shimizu, Prog. Theor. Phys. **74** (1985) 567 and **75** (1986) 905.
J. Fujimoto and M. Igarashi, Prog. Theor. Phys. **74** (1985) 791.
J. Fujimoto, M. Igarashi and Y. Shimizu, Prog. Theor. Phys. **77** (1987) 118.
[40] CELLO Collab., H.-J. Behrend et al., Phys. Lett. **B183** (1987) 400.
[41] M. Dine and J. Sapirstein, Phys. Rev. Lett. **43** (1979) 668;
K. G. Chetyrkin et al., Phys. Lett. **B85** (1979) 277;
W. Celmaster and R. J. Gonsalves, Phys. Rev. Lett. **44** (1980) 560.
[42] W. E. Caswell, Phys. Rev. Lett. **33** (1974) 244;
D. R. T. Jones, Nucl. Phys. **B75** (1974) 531;
A. A. Belavin and A. A. Migdal, JETP Lett. **19** (1974) 181.
[43] A. Sirlin, Phys. Rev. **D22** (1980) 971;
W. J. Marciano, Phys. Rev. **D20** (1979) 274;
M. Veltman, Phys. Lett. **B91** (1980) 95;
F. Antonelli et al., Phys. Lett. **B91** (1980) 90.
[44] W. J. Marciano and A. Sirlin, Phys. Rev. **D29** (1984) 945.